

Structural transformations during periodic deformation of low-porosity amorphous materials

Nikolai V. Priezjev^{1,2} and Maxim A. Makeev³

¹*Department of Mechanical and Materials Engineering,
Wright State University, Dayton, OH 45435*

²*National Research University Higher School of Economics, Moscow 101000, Russia and*

³*Department of Chemistry, University of Missouri-Columbia, Columbia, MO 65211*

(Dated: March 13, 2021)

Abstract

Atomistic simulations are employed to study structural evolution of pore ensembles in binary glasses under periodic shear deformation with varied amplitude. The consideration is given to porous systems in the limit of low porosity. The initial ensembles of pores are comprised of multiple pores with small sizes, which are approximately normally distributed. As periodic loading proceeds, the ensembles evolve into configurations with a few large-scale pores and significantly reduced number of small pores. These structural changes are reflected in the skewed shapes of the pore-size distribution functions and the appearance of a distinct peak at large length scales after hundreds of shear cycles. Moreover, periodic shear causes substantial densification of solid domains in the porous systems. The structural evolution of pore ensembles is found to stem from the formation of shear-band like regions of enhanced particle mobility after a number of transient cycles. The spatial extent of increased mobility depends strongly on the strain amplitude. A scaling theory is developed to qualitatively describe the transformation of the pore initial configurations of small-size voids into larger-scale void agglomerates.

PACS numbers: 34.20.Cf, 68.35.Ct, 81.05.Kf, 83.10.Rs

I. INTRODUCTION

The design of the optimal microstructural architecture for metallic glasses with enhanced ductility is important for various structural applications [1]. It is well recognized by now that homogeneous, pore-free metallic glasses yield via the formation of narrow shear bands leading to fracture and breaking of the material. However, the tensile ductility can be improved by spatially constraining shear bands and introducing porous heterostructures in an amorphous solid [1]. Thus, it was recently shown experimentally and numerically that a regular array of pores inside or at the surface of bulk metallic glasses changes the stress field upon deformation and guide the formation of shear bands along the domains with multiple pores [2, 3, 5, 6]. More recently, it was demonstrated that the strength of nanoporous metallic glasses depends sensitively on the porosity and pore shape, and the maximum strength is attained by localizing shear bands for sufficiently low values of porosity [7]. Using atomistic simulations, it was found that elastic moduli follow a power-law increase as a function of the average glass density in amorphous solids with random porous structures [8–11]. With further increasing strain, the porous structure deforms significantly and nearby pores tend to coalesce with each other leading to formation of a dominant cavity at high strain [8–11]. Nevertheless, the evolution of the pore size distribution and formation of shear bands in periodically deformed glasses still need to be thoroughly explored.

In the past few years, large-scale molecular dynamics simulations were extensively used to investigate the dynamic response of homogeneous amorphous materials to oscillatory shear deformation [12–28]. It was found that the relaxation dynamics at small strain amplitudes depends strongly on the preparation history. In particular, it was shown that after a few training cycles, slowly annealed glasses start to deform reversibly and the trajectory of each atom repeats itself at zero temperature [13, 14, 16, 17, 20]. Interestingly, during periodic deformation below yield, particles with relatively large displacements form clusters, which, depending on the strain amplitude, can be comparable to the system size [16]. On the other hand, poorly annealed glasses were found to relocate toward progressively lower potential energy levels when subjected to periodic loading in the elastic range [13, 21, 25–27]. The yielding transition typically occurs after a certain number of cycles, and it is accompanied by the formation of a system-spanning shear band in sufficiently large systems and, as a result, higher potential energy levels [21, 22, 26, 28]. Although some of these features, including

the decay of the potential energy and transient stress response, were recently detected in highly porous binary glasses under periodic shear [29], the exact mechanisms of the pore and glass phase redistribution as well as the nature of the yielding transition remain not fully understood.

In this paper, we use molecular dynamics simulations to investigate the effect of cyclic loading on evolution of porous structures in low-porosity binary glasses. We find that under periodic deformation, the initial ensemble of pores, which are approximately normally distributed, gradually evolve into configurations with a few large-scale pores that are energetically favorable. The structural transformations of the pore and glass phases are quantified via the pore-size and local density distribution functions. The results are rationalized by estimating the stability and lifetime of a pore, which depend on the pore size, surface energy, and strain-driven diffusion of atoms near the pore.

The paper is structured as follows. The details of molecular dynamics simulations including parameter values, interaction potentials, preparation and deformation protocols are provided in the next section. The time dependence of the potential energy series, variation of shear stress and analysis of pore size and local density distribution functions are presented in section III. The summary and concluding remarks are given in the last section.

II. DETAILS OF MD SIMULATIONS

In the present study, the molecular dynamics simulations were carried out on a model glass, which is represented by a binary (80:20) mixture first introduced by Kob and Andersen (KA) [30]. In the KA model, any two atoms of types $\alpha, \beta = A, B$ interact via the Lennard-Jones (LJ) potential of the form:

$$V_{\alpha\beta}(r) = 4\varepsilon_{\alpha\beta} \left[\left(\frac{\sigma_{\alpha\beta}}{r} \right)^{12} - \left(\frac{\sigma_{\alpha\beta}}{r} \right)^6 \right], \quad (1)$$

with the following parametrization $\varepsilon_{AA} = 1.0$, $\varepsilon_{AB} = 1.5$, $\varepsilon_{BB} = 0.5$, $\sigma_{AB} = 0.8$, and $\sigma_{BB} = 0.88$, and $m_A = m_B$ [30]. The LJ potential is truncated at the cutoff radius $r_{c,\alpha\beta} = 2.5\sigma_{\alpha\beta}$. As usual, we express physical quantities in the reduced LJ units of length, mass, energy, and time; namely, $\sigma = \sigma_{AA}$, $m = m_A$, $\varepsilon = \varepsilon_{AA}$, and $\tau = \sigma\sqrt{m/\varepsilon}$. The Newton's equations of motion for each atom were solved using the velocity-Verlet scheme [31] with the integration time step $\Delta t_{MD} = 0.005\tau$.

In order to obtain porous samples, we follow the preparation procedure introduced in the recent MD studies [33, 34]. First, the binary mixture of 300 000 particles was thoroughly equilibrated at constant volume and at the temperature of $1.5 \varepsilon/k_B$. Here, k_B stands for the Boltzmann constant. The glass transition temperature of the KA model is $T_g \approx 0.435 \varepsilon/k_B$ [30]. Second, the system was instantaneously quenched across the glass transition and allowed to evolve during the time interval of $10^4 \tau$ at constant volume and temperature $T_{LJ} = 0.05 \varepsilon/k_B$. As a result of the coarsening process and material solidification, the porous structure is developed in samples with the average glass density $\rho\sigma^3 = 0.9$.

After the porous structure was formed, the glass was subjected to periodic shear deformation at constant volume as follows:

$$\gamma(t) = \gamma_0 \sin(2\pi t/T), \quad (2)$$

where $\gamma(t)$ is time-dependent shear strain, γ_0 is the strain amplitude, $0 \leq \gamma_0 \leq 0.12$, and T is the oscillation period. In what follows, the period is fixed to $T = 500 \tau$, and the simulations were performed during 500 cycles for each value of the strain amplitude. To avoid ambiguity, we denote temperature by T_{LJ} , while the oscillation period is indicated by T . During periodic shear, the temperature $T_{LJ} = 0.05 \varepsilon/k_B$ was maintained via the Nosé-Hoover thermostat [32]. In addition, the so-called Lees-Edwards periodic boundary conditions were imposed along the plane of shear [31]. The MD simulations were performed only for one realization of disorder due to relatively large system size, which is required to avoid finite size effects [33, 34]. During production runs, several characteristics including potential energy, shear stress, and temperature, as well as positions of all atoms were periodically saved for the postprocessing analysis.

III. RESULTS

Before presenting our main results, we briefly revisit the dynamics of the coarsening process that leads to the formation of porous glassy media. As discussed in the recent MD studies [8–11, 29, 33–35], the binary mixture was first instantaneously quenched across the glass transition and then allowed to evolve freely at constant volume and $T_{LJ} = 0.05 \varepsilon/k_B$ during the time period of $10^4 \tau$. It was previously demonstrated that this time interval is sufficiently long, such that the typical size of solid domains crosses over to logarithmically

slow growth [33, 34]. It will be shown below, however, that in the absence of mechanical deformation, the porous structure undergoes a noticeable change during the subsequent time interval of $2.5 \times 10^5 \tau$. It should be pointed out that the essential feature of the coarsening process is the constraint of constant volume, which leads to built in tensile stresses and negative pressures [8, 33–35]. Thus, the average pressure was estimated to be $P \approx -0.73 \varepsilon / \sigma^3$ for porous samples with the average glass density $\rho \sigma^3 = 0.9$ and temperature $T_{LJ} = 0.05 \varepsilon / k_B$ [35].

The time dependence of the potential energy per atom for the indicated strain amplitudes is reported in Fig. 1 during 500 cycles. In each case, the potential energy continues to decrease over consecutive cycles, and, except for $\gamma_0 = 0.10$ and 0.12 , the minimum of the potential energy after 500 cycles becomes deeper with increasing strain amplitude. This trend is associated with significant rearrangement of the glass phase in the driven porous systems. Note that in the quiescent sample ($\gamma_0 = 0$), the decrease in the potential energy is less pronounced as it corresponds to the aging process at constant volume during the time interval $500 T = 2.5 \times 10^5 \tau$. Somewhat surprisingly, we observed that the potential energy for cyclic loading with $\gamma_0 = 0.10$ is lower than for $\gamma_0 = 0.12$. We attribute this behavior to the particular realization of disorder, which, upon cycling, resulted in larger pore structures and denser glass phase when $\gamma_0 = 0.10$ (discussed below). It should be mentioned that for all strain amplitudes, the potential energy levels are deeper for samples with the average glass density $\rho \sigma^3 = 0.9$ than for $\rho \sigma^3 = 0.5$ reported previously [29], even though only 500 cycles were applied in the former case and 2000 cycles in the latter case.

The variation of shear stress, σ_{xz} , as a function of time during 500 cycles is presented in Fig. 2 for different strain amplitudes. It can be seen that following about 50 transient cycles, the stress amplitude remains nearly constant. The relative trends, however, are distinctly different for the cases $\gamma_0 \leq 0.04$ and $\gamma_0 \geq 0.06$ during the first 50 cycles. At small strain amplitudes, $\gamma_0 \leq 0.04$, the stress amplitude gradually increases over the first 50 cycles, due to a rapid decrease of the potential energy, and then it saturates at a constant value corresponding to a nearly reversible, elastic deformation. A similar effect was observed for rapidly quenched, homogeneous binary glasses subjected to oscillatory shear deformation with strain amplitudes below yield [25, 26]. In contrast, the amplitude of stress oscillations at $\gamma_0 \geq 0.06$ decreases after a few cycles and becomes smaller than for the case $\gamma_0 = 0.04$,

indicating large-scale plastic deformation. These results are qualitatively similar to the behavior of shear stress for lower glass density samples $\rho\sigma^3 = 0.5$ reported in the previous study [29], although the magnitude of stress variations are significantly larger for the case $\rho\sigma^3 = 0.9$ presented herein.

A series of instantaneous snapshots of the porous glasses for selected strain amplitudes is illustrated in Figs. 3–8. In all panels, the snapshots are taken after the indicated number of cycles at zero strain. It can be observed that the porous structure remains nearly unchanged during 500 cycles for the quiescent sample shown in Fig. 3 and for the strain amplitude below the yield point, $\gamma_0 = 0.04$, see Fig. 4. While local plastic events are strongly suppressed in the quiescent glass at the low temperature $T_{LJ} = 0.05 \varepsilon/k_B$ (not shown), the collective irreversible displacements of atoms become abundant during the first several cycles at $\gamma_0 = 0.04$; however, they decay quickly over consecutive cycles, indicating nearly reversible shear deformation (see Fig. 9). This behavior is similar to the decrease in the volume occupied by atoms with large nonaffine displacements in quickly annealed, homogeneous binary glasses subjected to repetitive subyield cycling [25, 26].

In sharp contrast, periodic loading with large strain amplitudes, $\gamma_0 \geq 0.06$, results in significant redistribution of pores and formation of a dominant cavity after 500 cycles, see Figs. 5–8. As shown in Figs. 10 and 11, most of the atoms undergo large irreversible displacements during the first few transient cycles, followed by formation of a permanent shear band. Thus, the migration and coalescence of pores is enhanced in the regions populated with mobile atoms. It can be seen in Figs. 5 and 7 that pores are absent after 100 cycles inside the shear bands shown in Figs. 10 and 11. Note that similar trends are evident for other strain amplitudes, although they are not reported here for brevity. We also comment that the orientation of shear bands in Figs. 10 and 11 is perpendicular to the plane of shear. Such unusual orientation is related to the finite system size and a particular realization of disorder, and it was reported previously for periodically deformed binary glasses [22]. Finally, the transition from transient clusters to formation of a system-spanning shear band of large nonaffine displacements after a number of shear cycles was also observed for poorly annealed, homogeneous binary glasses [26].

In this work, the response behavior of the void-space networks to periodic loading is quantified by computing the pore size distribution (PSD) functions. The calculations of

the PSD functions were performed using the open source Zeo++ software [36–38]. The algorithmic structure of the code can be briefly described as follows. At the core of the implemented approach is the Voronoi tessellation, which allows for a translation of the microstructural information pertained to constituent atoms alongside with the geometrical characteristics of the periodic unit cell into a periodic graph representation of the void spaces between atoms. The connectivity of the void network, obtained thereby, is also computed. For each atom i , $i = 1, \dots, N$, in the system having neighbors $j = 1, \dots, N$, the Voronoi cell is defined by the following inequality $d(x, x_i) < d(x, x_j)$, where the distance $d(x, y)$ is the Euclidean distance between the x and y points in the space. In the Voronoi decomposition, the cells are defined as lines that are equidistant from three neighboring atoms. The Voronoi nodes are given by spatial positions, such that they are equidistant from four neighboring atoms. Thereby constructed edges and nodes provide a three-dimensional graph that represents the pores and channels. The nodes of the graph are given by the local maxima of the function $f(x) = \min\{d(x, x_i) : i = 1, \dots, N\}$. The specifics of implementation of the algorithm derive from a modified VORO++ software library, developed in Ref. [39]. As explicit in the foregoing, the computational tool provides all the essential information needed for complete characterization of a porous material system. That includes the surface areas of the pores and pore size distribution functions. In the former case, a Monte Carlo sampling is used for calculations, reported herein. In the present work, the number of samples per atom was fixed at 50000. The probe radius was chosen to be 0.3σ . As our studies show, the results are relatively insensitive to the probe radius, for probe-radius magnitudes less than 0.8σ .

The distributions of pore sizes during cyclic loading are reported in Fig. 12 for the strain amplitudes γ_0 : (a) 0.0, (b) 0.01, (c) 0.02, (d) 0.04, (e) 0.06, (f) 0.08, (g) 0.10, and (h) 0.12. It can be observed in Fig. 12 (a-b) that in the quiescent sample and periodically driven glass with the strain amplitude $\gamma_0 = 0.01$, the shape of the distribution functions remains nearly the same. With increasing strain amplitude below yielding transition, the pore size distributions become slightly skewed towards larger pore sizes, as shown in Fig. 12 (c-d). This observation correlates with the appearance of large-scale irreversible displacements during the first ten cycles in Fig. 9, which facilitate pore redistribution. The influence of cyclic loading on the shape of pore size distributions becomes significant for strain amplitudes $\gamma_0 \geq 0.06$. In particular, it can be seen that a dominant large-size pore is developed after

about 100 cycles, as shown in Fig. 12 (e-i). This trend is supported by visual observation of system snapshots in Figs. 5-8. Notice also the appearance of a high intensity peak after 500 cycles for $\gamma_0 = 0.10$ in Fig. 12 (h). The formation of a large cavity in Fig. 7 is reflected in the lowest potential energy minimum attained after 500 cycles with the strain amplitude $\gamma_0 = 0.10$ (see Fig. 1).

As explicit in the above, a periodic mechanical loading causes not only significant restructuring in the pore ensembles but also leads to significant atomic rearrangements in the solid domains. The latter effect was quantified by the corresponding studies of total energies, which are indicative of microstructural changes reminiscent of densification. To obtain a more quantitative atomistic-level picture of microstructural changes, we investigated the local density distribution in the solid domains. In the present study, the local density of solid domains, $\langle \rho \rangle_R$, is defined as the number of atoms located within the given radial dimension centered on a site of the cubic lattice $L \in R^3$. An analytical form for $\langle \rho \rangle_R$ can be obtained by employing the following procedure. For each site, i , of the lattice $\langle \rho \rangle_R$, we define a closed ball, $B_R = \{R \in \mathbb{R}^3, \sum_{j=1}^3 R_j^2 \leq R_0^2\}$, such that $R_0 = |\vec{R}_0|$ is a fixed non-zero rational number. In this case, on-site local densities for an microcanonical ensemble consisting of N atoms can be computed as $\langle \rho \rangle_R = 1/B_R \int dR^3 \delta(\vec{r}_i - \vec{R})$, where the integral is taken over B_R , and $i = 1, 2, \dots, N$ are the atomic indexes. The quantity $\langle \rho \rangle_R$ can be regarded as deviation of the local density from the average density of the system with homogeneous distribution of the solid phase.

In Fig. 13, we present the local density, $\langle \rho \rangle_R$, distribution functions, $\Pi(\langle \rho \rangle_R)$, computed for the porous systems under periodic loading with the strain amplitude, γ_0 : (a) 0.0, (b) 0.01, (c) 0.02, (d) 0.04, (e) 0.06, (f) 0.08, (g) 0.10, and (h) 0.12. The main focus here is on the effect of the strain amplitude on the structural changes taking place in the porous glassy materials. In our previous paper [29], we investigated the response of porous materials to periodic loading in the case of high porosity systems. The considered below case differs from the previously studied system in what related to both porosity and the form of the pore-size distribution function. The considered herein systems have low values of porosity and, correspondingly, Gaussian form of the pore-size distribution functions. Some of the observations, however, are similar to those, reported in Ref. [29]. Thus, in general, the periodic loading is found to cause substantial changes in density of the solid domains. Similar

to the previously considered case, the effects differ for densities, $\rho\sigma^3 < 0.5$, and densities close to the maximum, characteristic for the glass phase (density of homogeneous glass). It should also be noted that the effect of the strain amplitude is the same as the one unveiled for high-porosity systems. Indeed, we observed that the densification in the regions of high local density, $\rho\sigma^3 > 1.2$, is an increasing function of the strain amplitude. This observation holds for both the shift of the peak position to the range of larger densities and significant increase in the peak intensity. In the range of low densities, $\rho\sigma^3 < 0.5$, the magnitude of the intensity decreases. However, the intensity of the peak near $\rho\sigma^3 = 0.6$ is approximately preserved. It should be noted that the peak is due to the pore surface and originates from the near-surface atoms. The above observation is indicative that the total number of near-surface atoms remains nearly the same in the process of pore coalescence. This interesting observation requires additional studies focusing on thermodynamics of pore coalescence. The conclusions are similar to the case of lower density, considered in Ref. [29]. A periodic loading causes significant homogenization of the porous glasses. In the case considered herein, at large strain amplitudes, dynamical evolution of the pore structures leads to a formation of a single pore of large-size, and significant densification.

In Ref. [29], we investigated some dynamical aspects of the micropores evolution in porous glasses subjected to periodic shear deformation. The systems, considered therein, were characterized by a relatively large porosity, and the corresponding average density of the microporous material is $\rho\sigma^3 = 0.5$. As we have shown in Ref. [35], systems with large porosity demonstrate both rather complex pore-size distributions and highly non-trivial topology of micropores involving isolated micropore structures and channels. On the other hand, at higher densities, the pore configurations primarily consist of separated by relatively large distances micropores and their sizes are distributed according to a Gaussian. As was noted in Ref. [35], the Gaussian ensembles of pores are characteristic for dense glassy systems, as has been previously observed in experimental studies [40, 41]. The transition to the regime characterized by the Gaussian distribution has also been discussed in detail in Ref. [35]. One of the key observations of the present study is the apparent distinction between changes in the structure of micropore ensembles in systems with high (see Ref. [29]) and low porosity.

With some restrictions, we can define a low-porosity system, as a system that shows a Gaussian distribution of pore-sizes. In such systems, the large amplitude loading leads to a

formation of large micropores, accompanied by annihilation of the small ones via diffusion-driven coalescence. As we show below, this behavior can be explained on the basis of a simple theoretical framework. To this end, let us consider a system comprised of two pores in a glassy medium. An illustration of the problem under consideration is given in Fig. 14. Note that, in general, the problem of pore coalescence is rather complex and involves elastic interaction between pores, matrix material properties dependence on porosity, and spatial position-dependent chemical potential. In what follows, we present a simplified theory, which, however, describes well the underlying mechanism of micropore coalescence. As shown in Fig. 14, we consider two micropores, separated by radial distance r . The chemical potential of an atom in the bulk of solid materials is defined as μ_0 and the chemical potential of atoms in close vicinity of the two pores are denoted as μ_a and μ_n , respectively. To approximate the chemical potential, we employ the Kelvin's equation [42]:

$$\mu = \mu_0 + \Omega \sigma_s / r_s, \quad (3)$$

where Ω is the atomic volume, σ_s is the surface tension, and r_s is the radius of pore's curvature. If the pore closure is fully defined by mass transfer, the lifetime of the pore is given by $\tau_\ell \sim S_s / J \sim R_p^2 / J$, where S_s is the initial pore area and J is the current into the pore; the latter is related to the current density, j , and surface area of the pore, S_s , by $J = j S_s$. In turn, the current density, j , is related to the chemical potential, given by Eq. (3), as:

$$j = -\frac{D_T c}{k_B T} \nabla \mu, \quad (4)$$

where c is the concentration, T is temperature, and D_T in our case is the local strain-induced diffusion coefficient that reflects the enhanced mobility of atoms in shear bands. Next, we approximate Eq. (4) by the following expression:

$$j = \frac{D_T c}{k_B T} (\mu_a - \mu_n) / r, \quad (5)$$

where μ_a is the approximation for the chemical potential of atoms near the micropore under consideration using Eq. (3) and μ_n is the approximation for the chemical potential of atoms a neighboring micropore or sample surface (see Fig. 14). Note that in both cases – that is, a neighboring pore and the sample surface, the chemical potential is defined by the curvature. For some realizations of the pore geometries, a big pore can be regarded as nearly flat surface and therefore the existence of sample surface can be disregarded if the pore closure

is due to a growth of a neighboring pore. Let us omit all the external stress fields and consider a case, when the chemical potential is defined largely by the surface tension. The model is supported by a number of observations, presented in foregoing discussion. First, the pore coalescence leads to a decrease in potential energy and thus corresponds to an energetically more favorable configuration (see Fig. 1). Second, periodic deformation induces an enhanced diffusivity in large-scale domains, as shown in Figs. 9–11. This observation supports the assumption that the mass transfer into pores occurs in regions where the pore surface intersects a shear band. In the following, we restrict ourselves to the classical Kelvin’s problem, Eq. (3). In this case, the chemical potential is fully defined by the curvature of the pore via Eq. (3). Correspondingly,

$$\mu_a - \mu_n \sim S_s \sigma_s (1/R_s - 1/R_n). \quad (6)$$

Using Eq. (6), we readily arrive at the following expression for the lifetime, τ_ℓ :

$$\tau_\ell \sim \frac{k_B T}{D_{TC} \sigma_s} \frac{R_s^2 r}{1 - R_s/R_n}. \quad (7)$$

The theoretical framework, developed above, derives from the original ideas, put forth by Herring in Ref. [43]. A number of interesting conclusions can be deduced from the above formula. For example, systems comprised of a pair of micropores of the same geometry remain stable. This is not what we observe in our simulations. The discrepancy is due to the fact that the instability in our model systems is caused by the externally applied loading. An extension of the model is needed to include all the relevant stress fields. Next observation is that the micropore lifetime is an increasing function of its radius. This finding is consistent with our observation that small micropores are less stable compared to their counterparts having larger dimensions. Also, an increase in diffusivity makes the pore lifetime shorter, as Eq. (7) predicts the inverse linear dependence on the diffusion coefficient. Note that Eq. (7) provides only a crude approximation to the processes taking place during micropore ensembles reorganization. It appears, however, that it can be a good starting point for developing a deeper theoretical understanding of the phenomenon under consideration.

IV. CONCLUSIONS

In summary, we investigated the structural transformation and dynamic response of microporous glassy materials to periodic shear deformation using molecular dynamics simula-

tions. We found that periodic loading leads to a significant reorganization in the structure of both void patterns and density of solid domains. The nature of reorganization and its extent both depend strongly on the strain amplitude and the number of loading cycles. Moreover, the structural rearrangements of micropores in periodically driven systems are associated with a gradual transition to lower energy states. The observed changes in the potential energy are attributed to a decrease in the pore surface energy, taking place due to micropores coalescence into voids with significantly larger dimensions and densification of the solid domains. The two observations are quantified by computing the pore-size and local density distribution functions; the former accounts for the void-spaces evolution and the latter for the density of solid domains.

Furthermore, we showed that periodic deformation leads to enhanced mobility of atoms in the whole system during the transient cycles, which are followed by the formation of permanent shear bands at sufficiently large strain amplitudes. We identified and quantified the effects of increased mobility by computing the atomic displacements and separated the atoms into groups based upon their displacements during each cycle. In addition, we found that the temporal evolution of the micropore ensembles from the initial configurations of small-size pores into larger-scale agglomerates is facilitated by the strain-induced diffusion of atoms in extended domains of high mobility. Based upon assumption of strain-activated nature of the micropore evolution, we developed an approximate expression for the pore lifetime depending on its size and surface energy. Despite its simplicity, the scaling analysis correctly captures the key findings regarding the pore coalescence deduced from the atomistic simulations.

Acknowledgments

Financial support from the National Science Foundation (CNS-1531923) is gratefully acknowledged. The article was prepared within the framework of the Basic Research Program at the National Research University Higher School of Economics (HSE) and supported within the framework of a subsidy by the Russian Academic Excellence Project ‘5-100’. The molecular dynamics simulations were performed using the LAMMPS code [32]. The distributions of pore sizes were computed using the open-source software ZEO++ developed at the Lawrence Berkeley National Laboratory [36–38]. Computational work in support of this

research was performed at Wright State University's High Performance Computing Facility and the Ohio Supercomputer Center.

- [1] B. Sarac and J. Schroers, Designing tensile ductility in metallic glasses, *Nat. Commun.* **4**, 2158 (2013).
- [2] B. Sarac, B. Klusemann, T. Xiao, and S. Bargmann, Materials by design: An experimental and computational investigation on the microanatomy arrangement of porous metallic glasses, *Acta Mater.* **77**, 411 (2014).
- [3] M. Gao, J. Dong, Y. Huan, Y. T. Wang, and W.-H. Wang, Macroscopic tensile plasticity by scalarizing stress distribution in bulk metallic glass, *Sci. Rep.* **6**, 21929 (2016).
- [4] D. Sopu, C. Soyarslan, B. Sarac, S. Bargmann, M. Stoica, and J. Eckert, Structure-property relationships in nanoporous metallic glasses, *Acta Mater.* **106**, 199 (2016).
- [5] H. Y. Song, S. Li, Y. G. Zhang, Q. Deng, T. H. Xu, and Y. L. Li, Atomic simulations of plastic deformation behavior of $\text{Cu}_{50}\text{Zr}_{50}$ metallic glass, *J. Non-Cryst. Solids* **471**, 312 (2017).
- [6] Y. Luo, G. Yang, Y. Shao, and K. Yao, The effect of void defects on the shear band nucleation of metallic glasses, *Intermetallics* **94**, 114 (2018).
- [7] X. Zhou, L. Wang, and C. Q. Chen, Strengthening mechanisms in nanoporous metallic glasses, *Comput. Mater. Sci.* **155**, 151 (2018).
- [8] N. V. Priezjev and M. A. Makeev, Evolution of the pore size distribution in sheared binary glasses, *Phys. Rev. E* **96**, 053004 (2017).
- [9] N. V. Priezjev and M. A. Makeev, Strain-induced deformation of the porous structure in binary glasses under tensile loading, *Comput. Mater. Sci.* **150**, 134 (2018).
- [10] N. V. Priezjev and M. A. Makeev, Structural relaxation of porous glasses due to internal stresses and deformation under tensile loading at constant pressure, *arXiv:1808.04033* (2018).
- [11] N. V. Priezjev and M. A. Makeev, Structural transformations and mechanical properties of porous glasses under compressive loading, *J. Non-Cryst. Solids* (2018). In press. DOI: <https://doi.org/10.1016/j.jnoncrysol.2018.04.008>
- [12] N. V. Priezjev, Heterogeneous relaxation dynamics in amorphous materials under cyclic loading, *Phys. Rev. E* **87**, 052302 (2013).
- [13] D. Fiocco, G. Foffi, and S. Sastry, Oscillatory athermal quasistatic deformation of a model

- glass, Phys. Rev. E **88**, 020301(R) (2013).
- [14] I. Regev, T. Lookman, and C. Reichhardt, Onset of irreversibility and chaos in amorphous solids under periodic shear, Phys. Rev. E **88**, 062401 (2013).
 - [15] N. V. Priezjev, Dynamical heterogeneity in periodically deformed polymer glasses, Phys. Rev. E **89**, 012601 (2014).
 - [16] I. Regev, J. Weber, C. Reichhardt, K. A. Dahmen, and T. Lookman, Reversibility and criticality in amorphous solids, Nat. Commun. **6**, 8805 (2015).
 - [17] N. V. Priezjev, Reversible plastic events during oscillatory deformation of amorphous solids, Phys. Rev. E **93**, 013001 (2016).
 - [18] T. Kawasaki and L. Berthier, Macroscopic yielding in jammed solids is accompanied by a non-equilibrium first-order transition in particle trajectories, Phys. Rev. E **94**, 022615 (2016).
 - [19] Y. F. Ye, S. Wang, J. Fan, C. T. Liu, and Y. Yang, Atomistic mechanism of elastic softening in metallic glass under cyclic loading revealed by molecular dynamics simulations, Intermetallics **68**, 5 (2016).
 - [20] N. V. Priezjev, Nonaffine rearrangements of atoms in deformed and quiescent binary glasses, Phys. Rev. E **94**, 023004 (2016).
 - [21] P. Leishangthem, A. D. S. Parmar, and S. Sastry, The yielding transition in amorphous solids under oscillatory shear deformation, Nat. Commun. **8**, 14653 (2017).
 - [22] N. V. Priezjev, Collective nonaffine displacements in amorphous materials during large-amplitude oscillatory shear, Phys. Rev. E **95**, 023002 (2017).
 - [23] S. Dagois-Bohy, E. Somfai, B. P. Tighe, and M. van Hecke, Softening and yielding of soft glassy materials, Soft Matter **13**, 9036 (2017).
 - [24] R. Ranganathan, Y. Shi, and P. Koblinski, Commonalities in frequency-dependent viscoelastic damping in glasses in the MHz to THz regime, J. Appl. Phys. **122**, 145103 (2017).
 - [25] N. V. Priezjev, Molecular dynamics simulations of the mechanical annealing process in metallic glasses: Effects of strain amplitude and temperature, J. Non-Cryst. Solids **479**, 42 (2018).
 - [26] N. V. Priezjev, The yielding transition in periodically sheared binary glasses at finite temperature, Comput. Mater. Sci. **150**, 162 (2018).
 - [27] N. V. Priezjev, Slow relaxation dynamics in binary glasses during stress-controlled, tension-compression cyclic loading, Comput. Mater. Sci. **153**, 235 (2018).
 - [28] A. D. S. Parmar, S. Kumar, and S. Sastry, Strain localisation above the yielding point in

- cyclically deformed glasses, arXiv:1806.02464 (2018).
- [29] N. V. Priezjev and M. A. Makeev, The influence of periodic shear on structural relaxation and pore redistribution in binary glasses, arXiv:1808.09323 (2018).
 - [30] W. Kob and H. C. Andersen, Testing mode-coupling theory for a supercooled binary Lennard-Jones mixture: The van Hove correlation function, *Phys. Rev. E* **51**, 4626 (1995).
 - [31] M. P. Allen and D. J. Tildesley, *Computer Simulation of Liquids* (Clarendon, Oxford, 1987).
 - [32] S. J. Plimpton, Fast parallel algorithms for short-range molecular dynamics, *J. Comp. Phys.* **117**, 1 (1995).
 - [33] V. Testard, L. Berthier, and W. Kob, Influence of the glass transition on the liquid-gas spinodal decomposition, *Phys. Rev. Lett.* **106**, 125702 (2011).
 - [34] V. Testard, L. Berthier, and W. Kob, Intermittent dynamics and logarithmic domain growth during the spinodal decomposition of a glass-forming liquid, *J. Chem. Phys.* **140**, 164502 (2014).
 - [35] M. A. Makeev and N. V. Priezjev, Distributions of pore sizes and atomic densities in binary mixtures revealed by molecular dynamics simulations, *Phys. Rev. E* **97**, 023002 (2018).
 - [36] D. Ongari, P. G. Boyd, S. Barthel, M. Witman, M. Haranczyk, and B. Smit, Accurate characterization of the pore volume in microporous crystalline materials, *Langmuir* **33**, 14529 (2017).
 - [37] R. L. Martin, B. Smit, and M. Haranczyk, Addressing challenges of identifying geometrically diverse sets of crystalline porous materials, *J. Chem. Inf. Model.* **52**, 308 (2012).
 - [38] T. F. Willems, C. H. Rycroft, M. Kazi, J. C. Meza, and M. Haranczyk, Algorithms and tools for high-throughput geometry-based analysis of crystalline porous materials, *Micropor. Mesopor. Mater.* **149**, 134 (2012).
 - [39] C. H. Rycroft, VORO++: A three-dimensional Voronoi cell library in C++, *Chaos* **19**, 041111 (2009).
 - [40] A. R. Yavari, A. Le Moulec, A. Inoue, N. Nishiyama, N. Lupu, E. Matsubara, W. J. Botta, G. Vaughan, M. Di Michiel, and A. Kvick, Excess free volume in metallic glasses measured by X-ray diffraction, *Acta Mater.* **53**, 1611 (2005).
 - [41] G. Dlubek, A. P. Clarke, H. M. Fretwell, S. B. Dugdale, and M. A. Alam, Positron lifetime studies of free volume hole size distribution in glassy polycarbonate and polystyrene, *Phys. Stat. Sol. (A)* **157**, 351 (1996).

- [42] W. Thomson, On the equilibrium of vapour at a curved surface of liquid, Philosophical Magazine **42**, 448-452 (1871).
- [43] C. Herring, Effect of change of scale on sintering phenomena, J. Appl. Phys. **21**, 301 (1950).

Figures

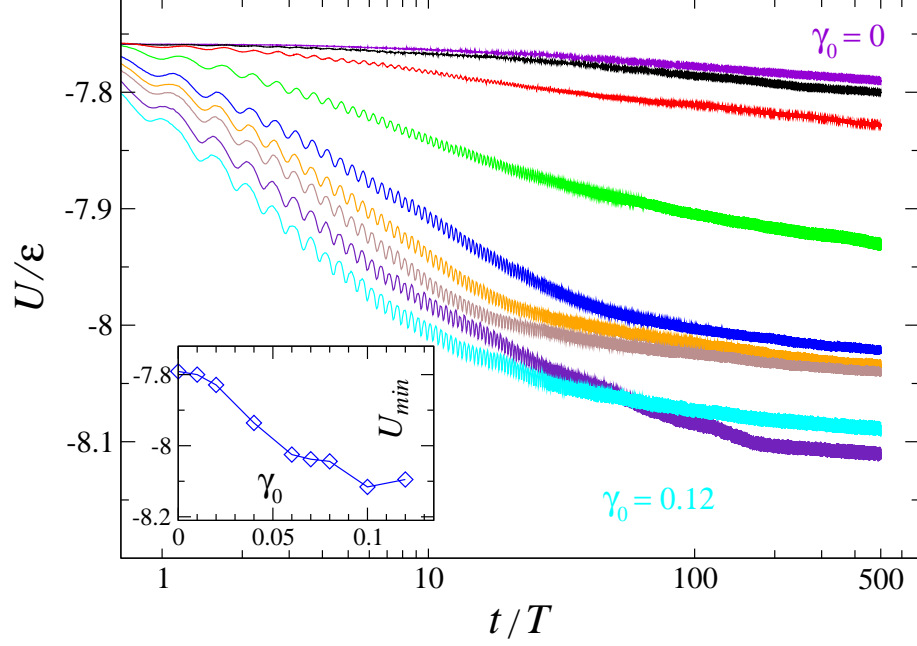


FIG. 1: (Color online) The potential energy, U , as a function of time for strain amplitudes $\gamma_0 = 0, 0.01, 0.02, 0.04, 0.06, 0.07, 0.08, 0.10$, and 0.12 (from top to bottom). The average glass density is $\rho\sigma^3 = 0.9$ and the oscillation period is $T = 500\tau$. The inset shows the variation of U after 500 cycles versus the strain amplitude.

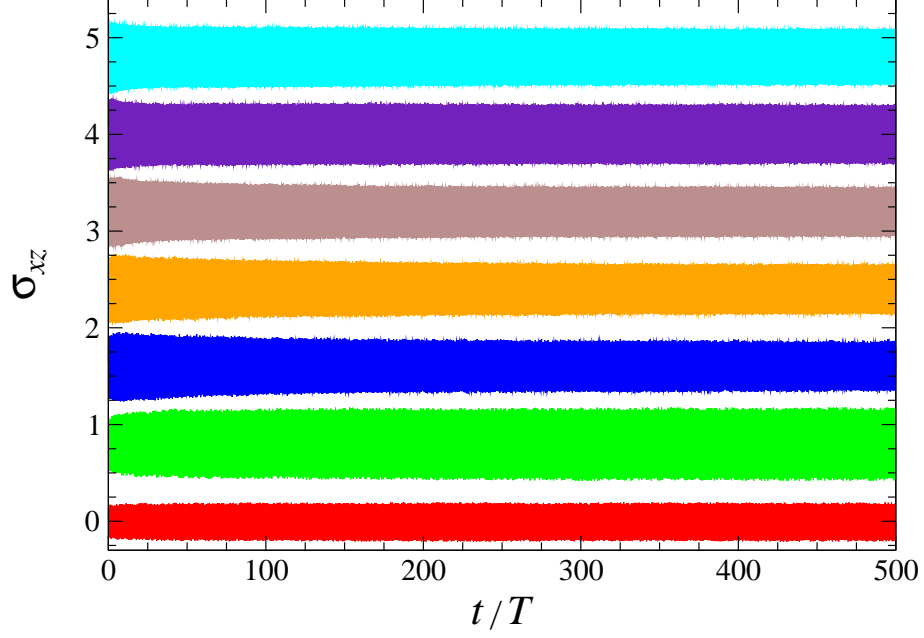


FIG. 2: (Color online) The time-dependent shear stress σ_{xz} (in units of $\varepsilon\sigma^{-3}$) for strain amplitudes $\gamma_0 = 0.02, 0.04, 0.06, 0.07, 0.08, 0.10$, and 0.12 (from bottom to top). The data are displaced upward by $0.8\varepsilon\sigma^{-3}$ for $\gamma_0 = 0.04$, by $1.6\varepsilon\sigma^{-3}$ for $\gamma_0 = 0.06$, by $2.4\varepsilon\sigma^{-3}$ for $\gamma_0 = 0.07$, by $3.2\varepsilon\sigma^{-3}$ for $\gamma_0 = 0.08$, by $4.0\varepsilon\sigma^{-3}$ for $\gamma_0 = 0.10$, and by $4.8\varepsilon\sigma^{-3}$ for $\gamma_0 = 0.12$.

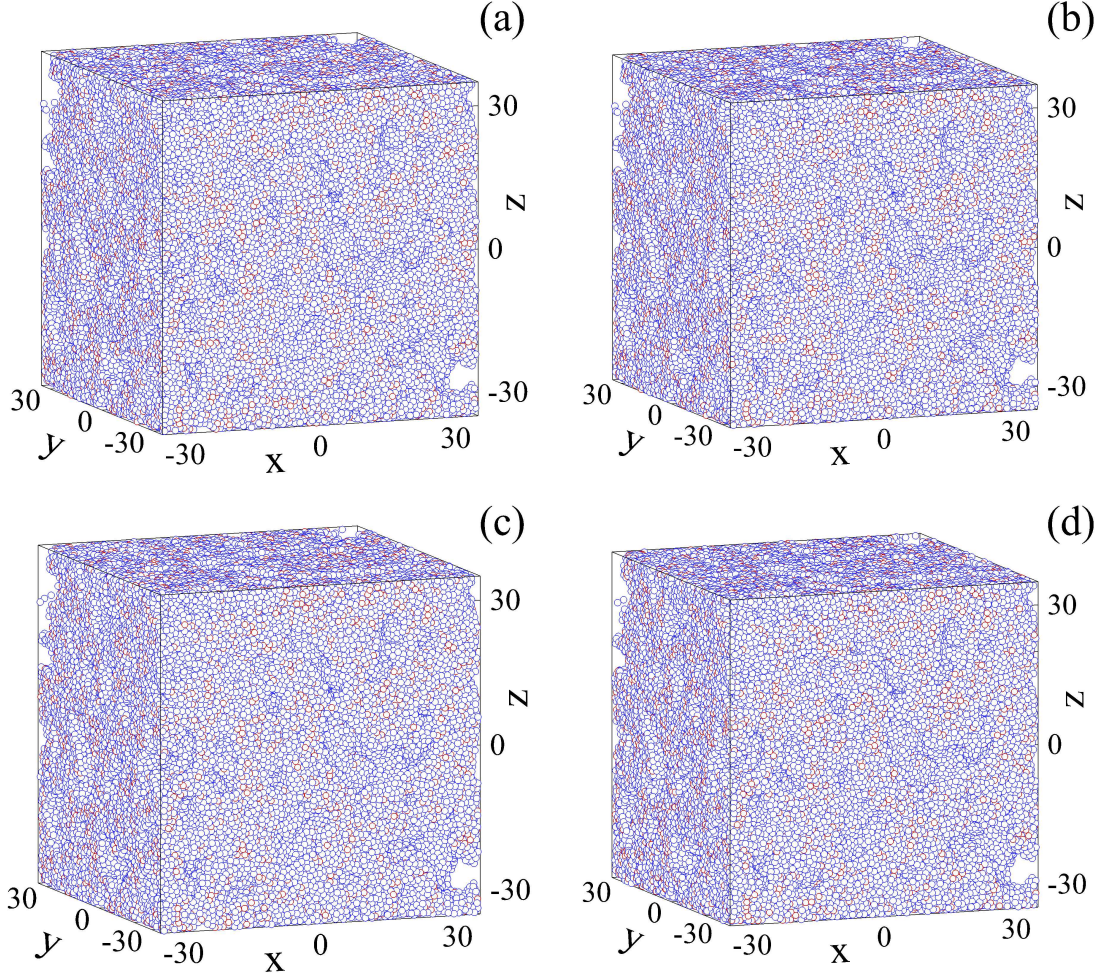


FIG. 3: (Color online) Consecutive snapshots of the quiescent glass ($\gamma_0 = 0$) after the time intervals (a) T , (b) $10T$, (c) $100T$, and (d) $500T$. The oscillation period is $T = 500\tau$ and the average glass density is $\rho\sigma^3 = 0.9$.

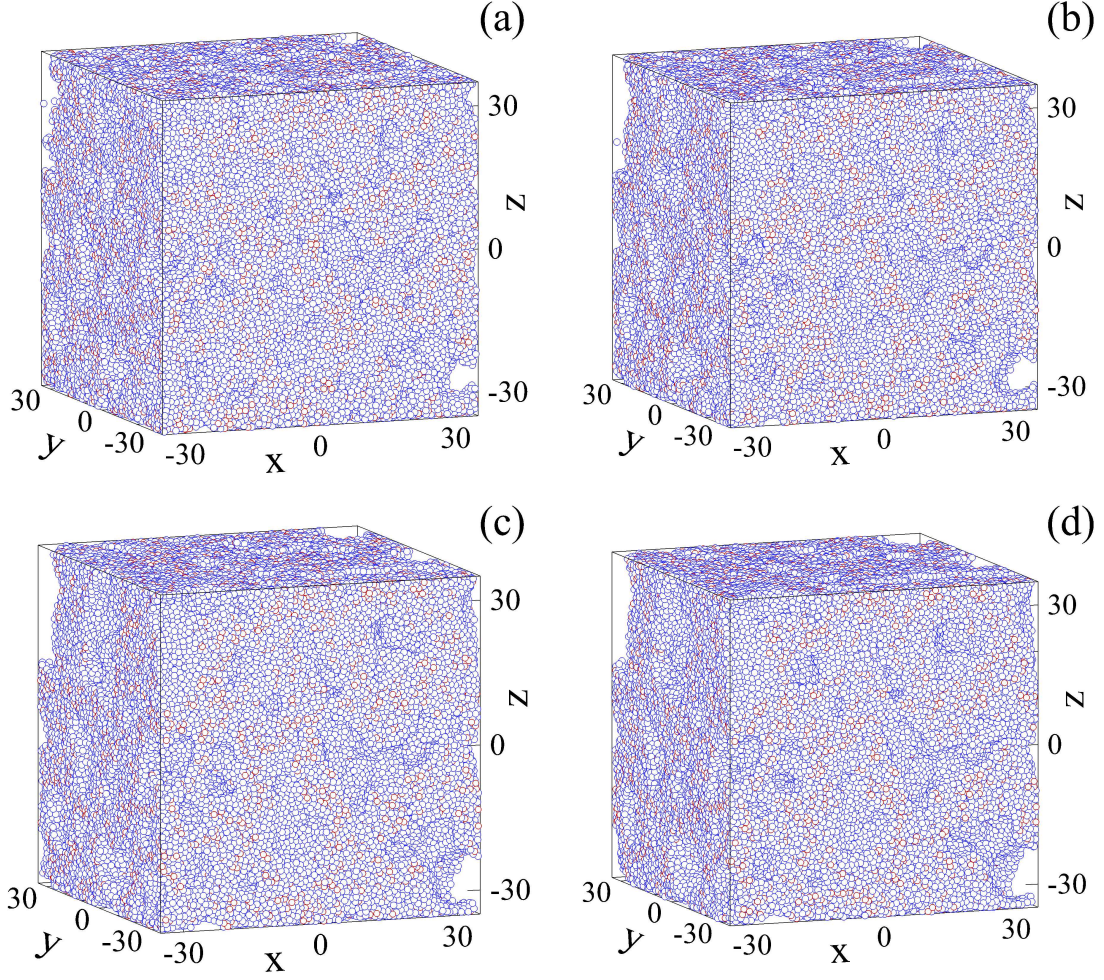


FIG. 4: (Color online) System snapshots during periodic deformation with the strain amplitude $\gamma_0 = 0.04$ after (a) 1-st, (b) 10-th, (c) 100-th, and (d) 500-th cycle at zero strain.

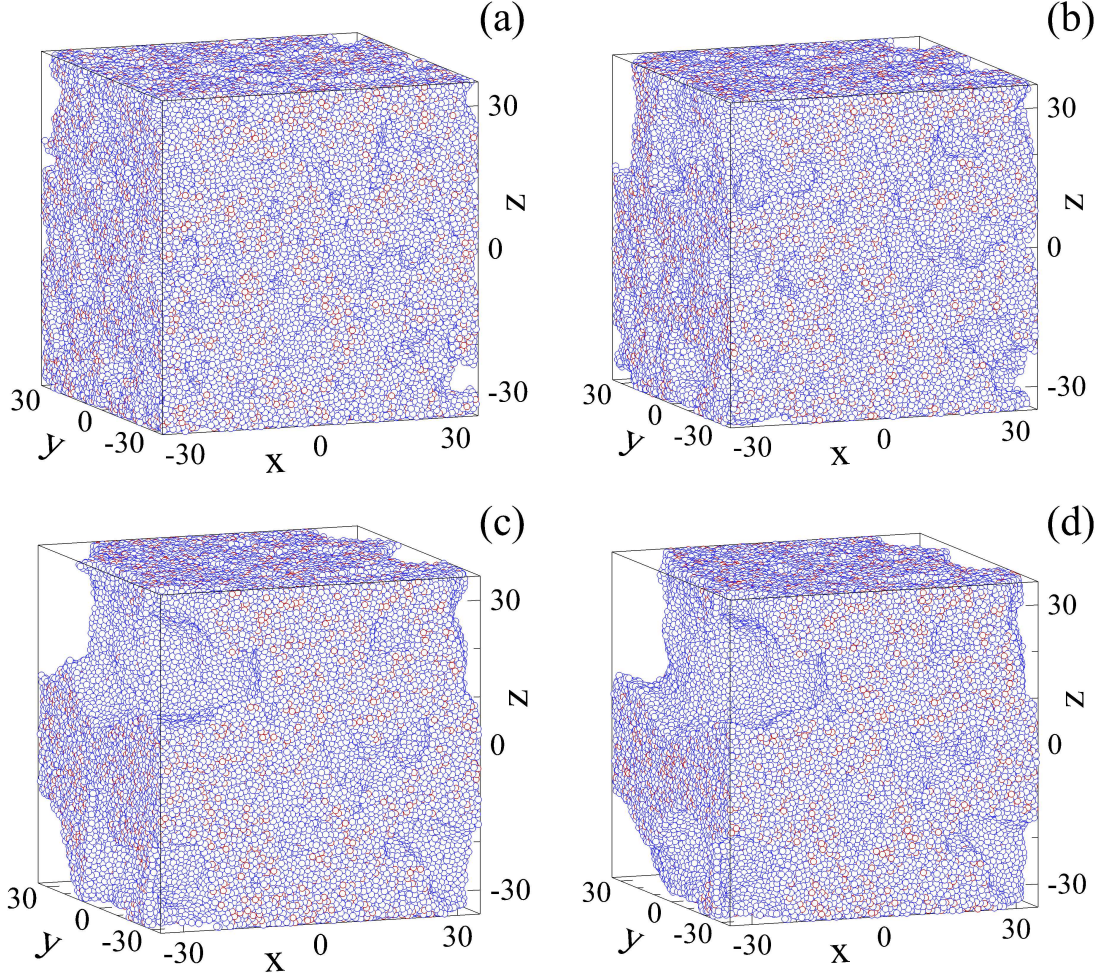


FIG. 5: (Color online) Spatial configurations of atoms during oscillatory shear deformation with the strain amplitude $\gamma_0 = 0.06$ after (a) 1-st, (b) 10-th, (c) 100-th, and (d) 500-th cycle.

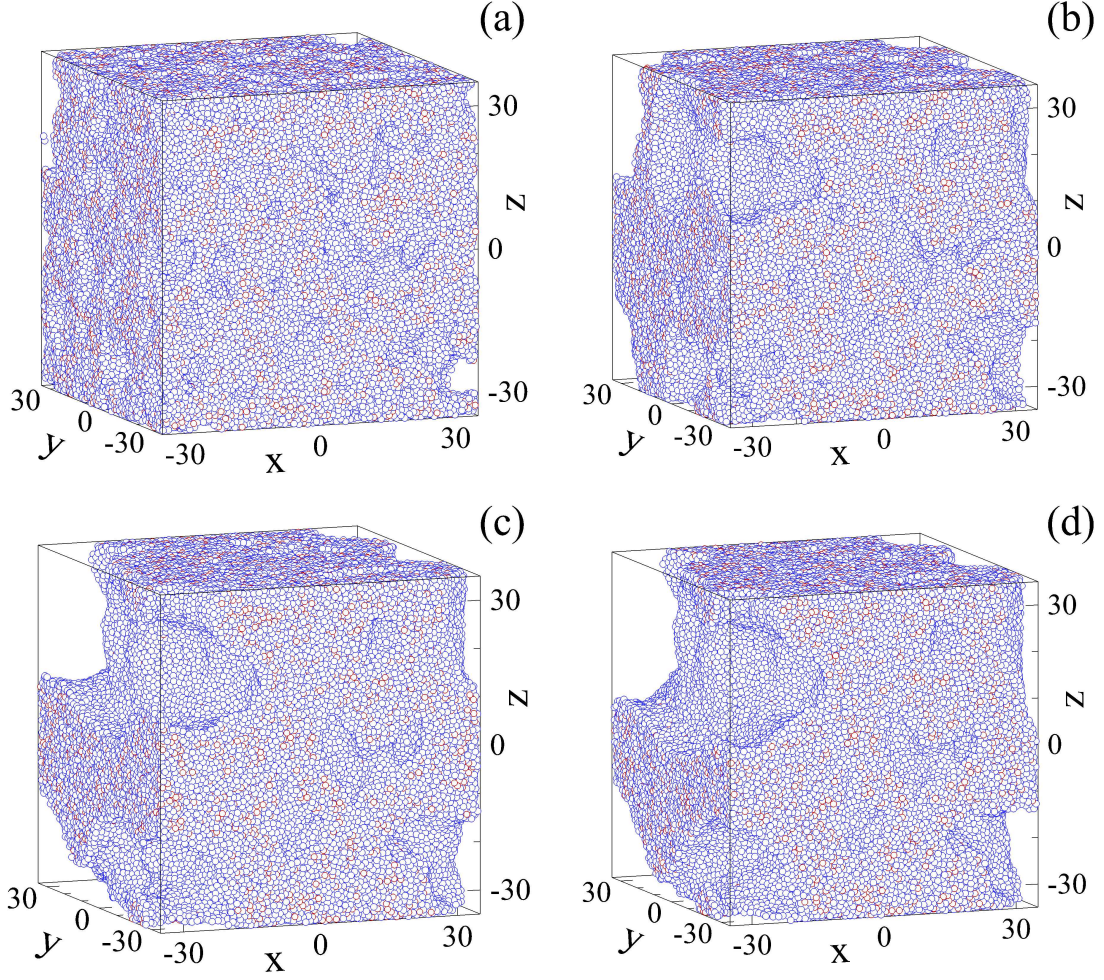


FIG. 6: (Color online) Atom positions at zero strain during periodic loading with the strain amplitude $\gamma_0 = 0.08$ after (a) 1-st, (b) 10-th, (c) 100-th, and (d) 500-th cycle.

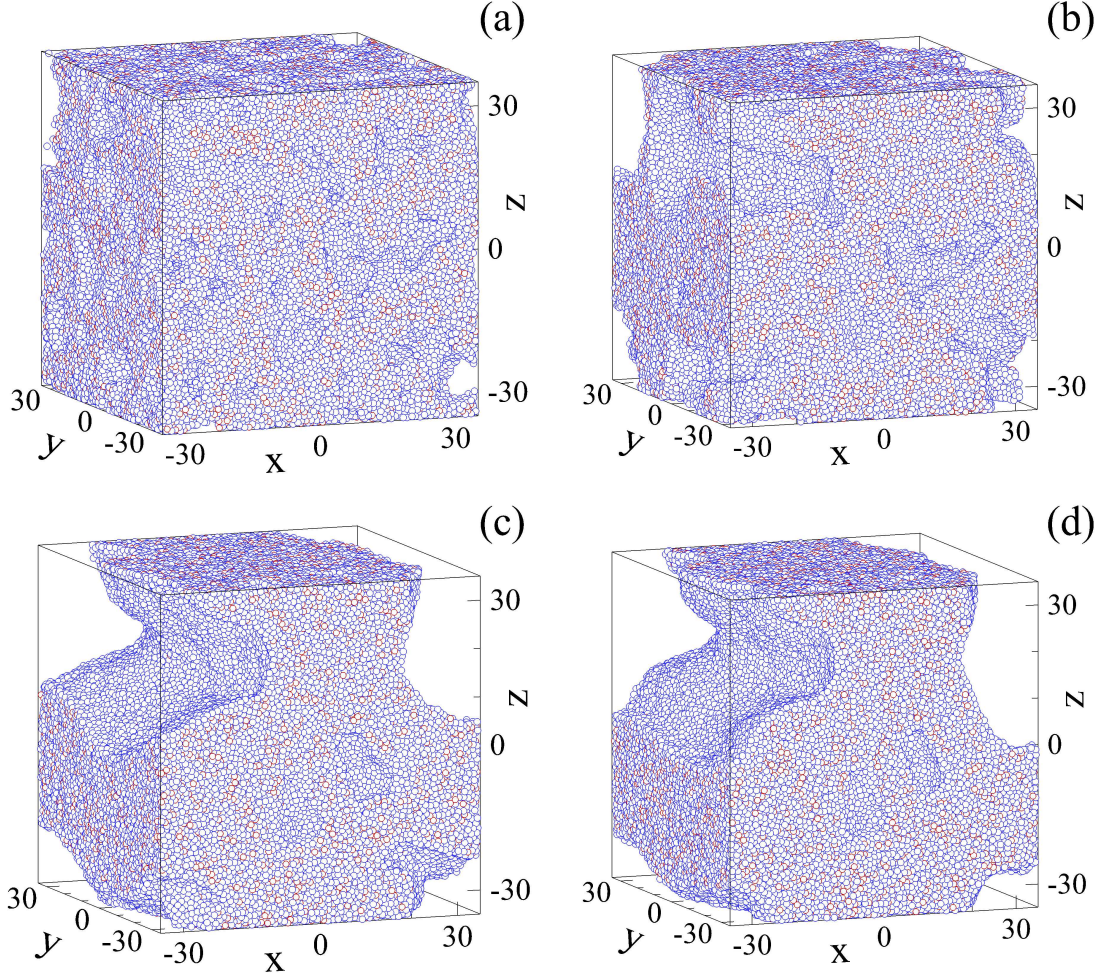


FIG. 7: (Color online) Instantaneous snapshots of the porous glass during cyclic loading with the strain amplitude $\gamma_0 = 0.10$ after (a) 1-st, (b) 10-th, (c) 100-th, and (d) 500-th cycle.

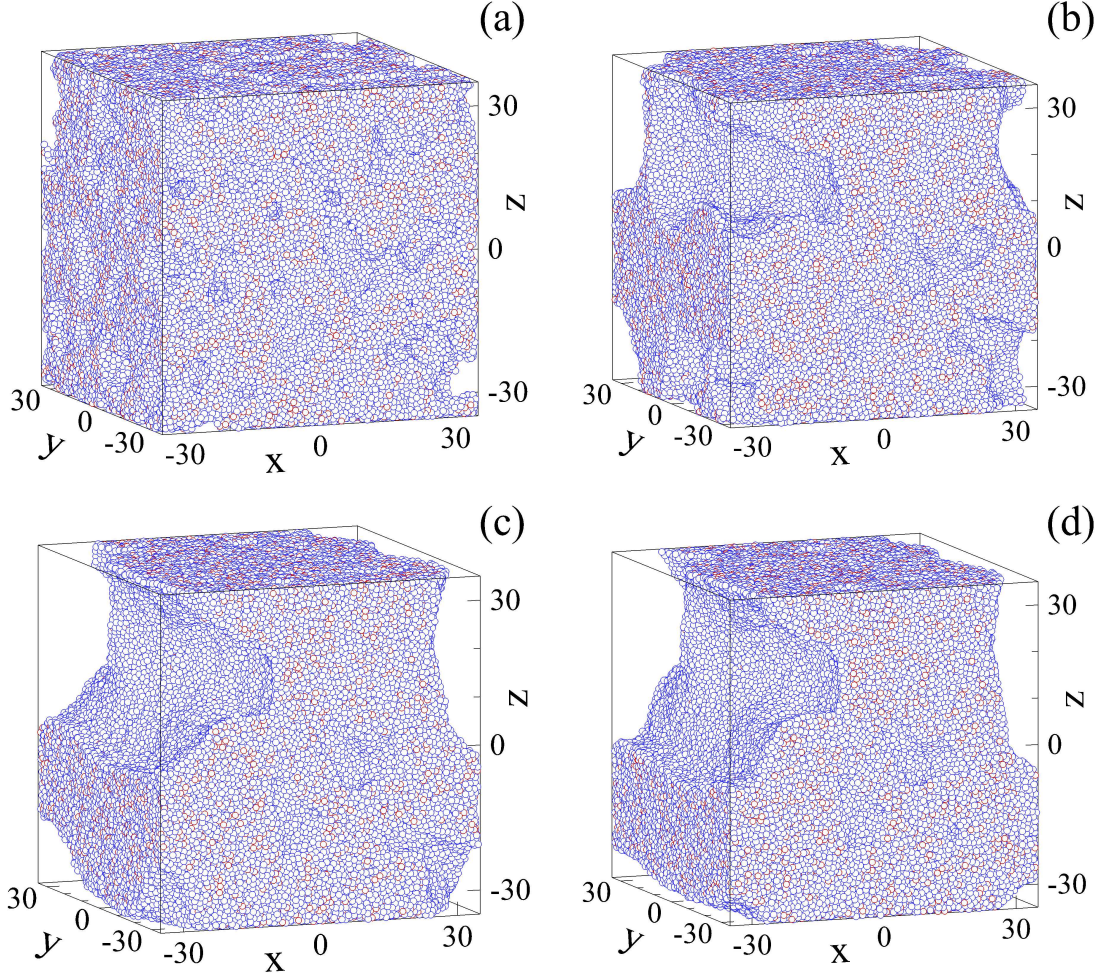


FIG. 8: (Color online) Atomic configurations during cyclic shear deformation with the strain amplitude $\gamma_0 = 0.12$ after (a) 1-st, (b) 10-th, (c) 100-th, and (d) 500-th cycle.

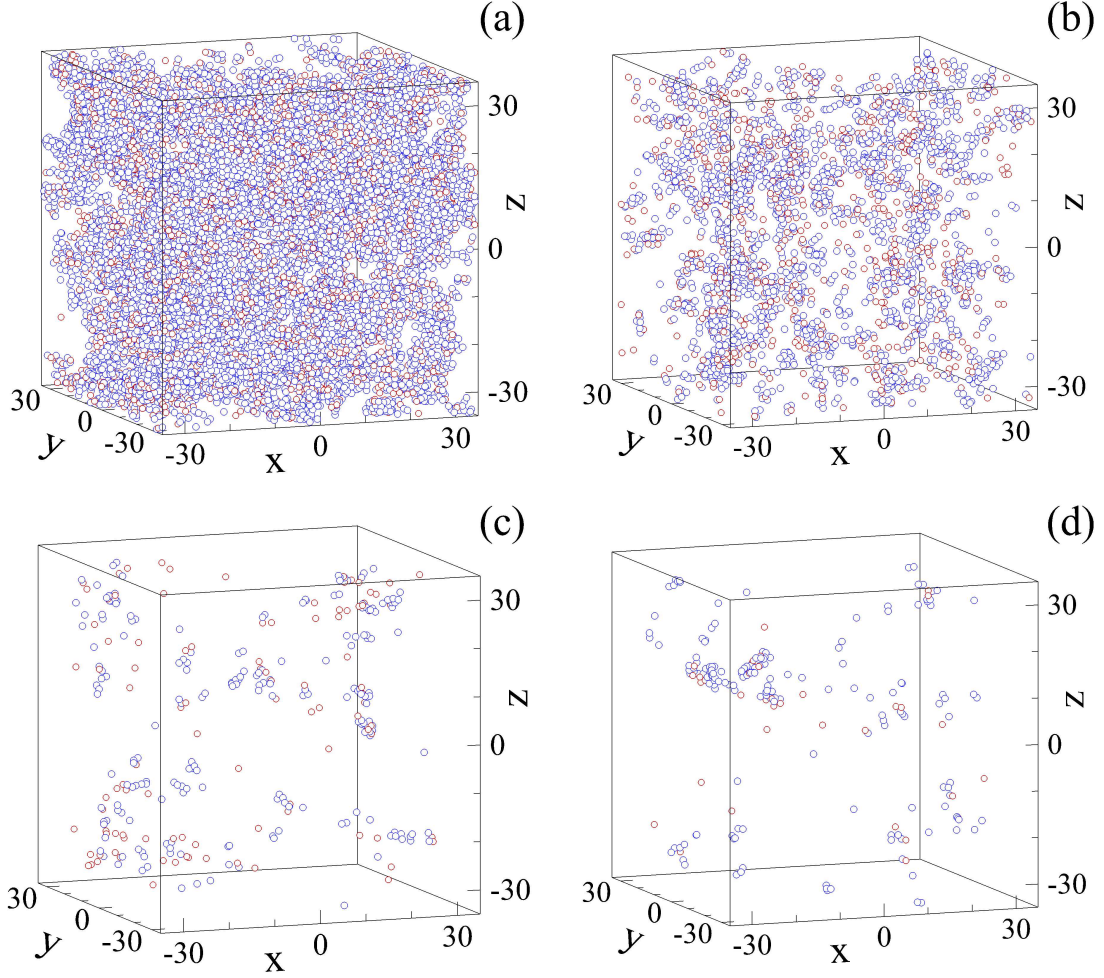


FIG. 9: (Color online) The positions of atoms whose displacements during one cycle is greater than 0.6σ for the cycle numbers (a) 1, (b) 10, (c) 100, and (d) 500. The strain amplitude is $\gamma_0 = 0.04$. The same data as in Fig. 4.

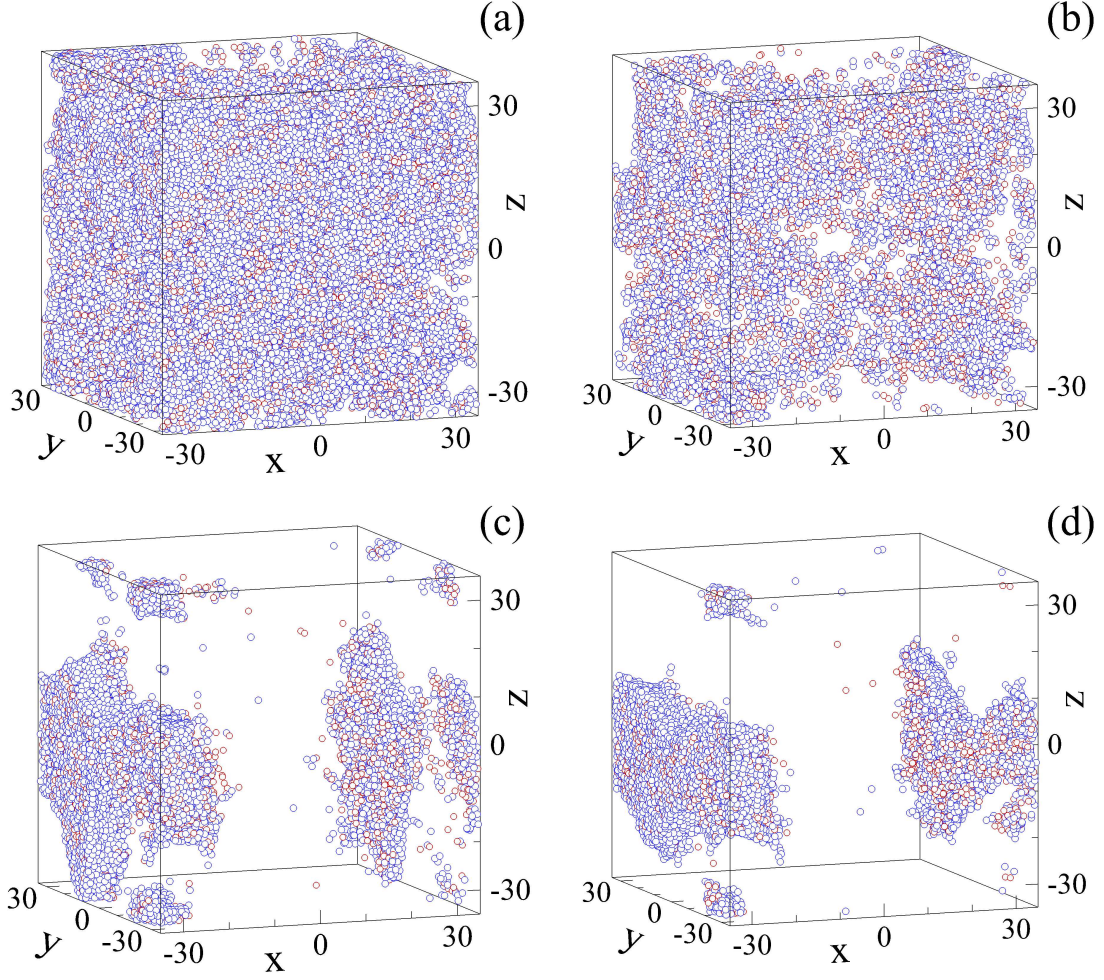


FIG. 10: (Color online) Configurations of atoms with displacements during one back-and-forth cycle greater than 0.6σ for the cycle numbers (a) 1, (b) 10, (c) 100, and (d) 500. The strain amplitude is $\gamma_0 = 0.06$. The same data as in Fig. 5.

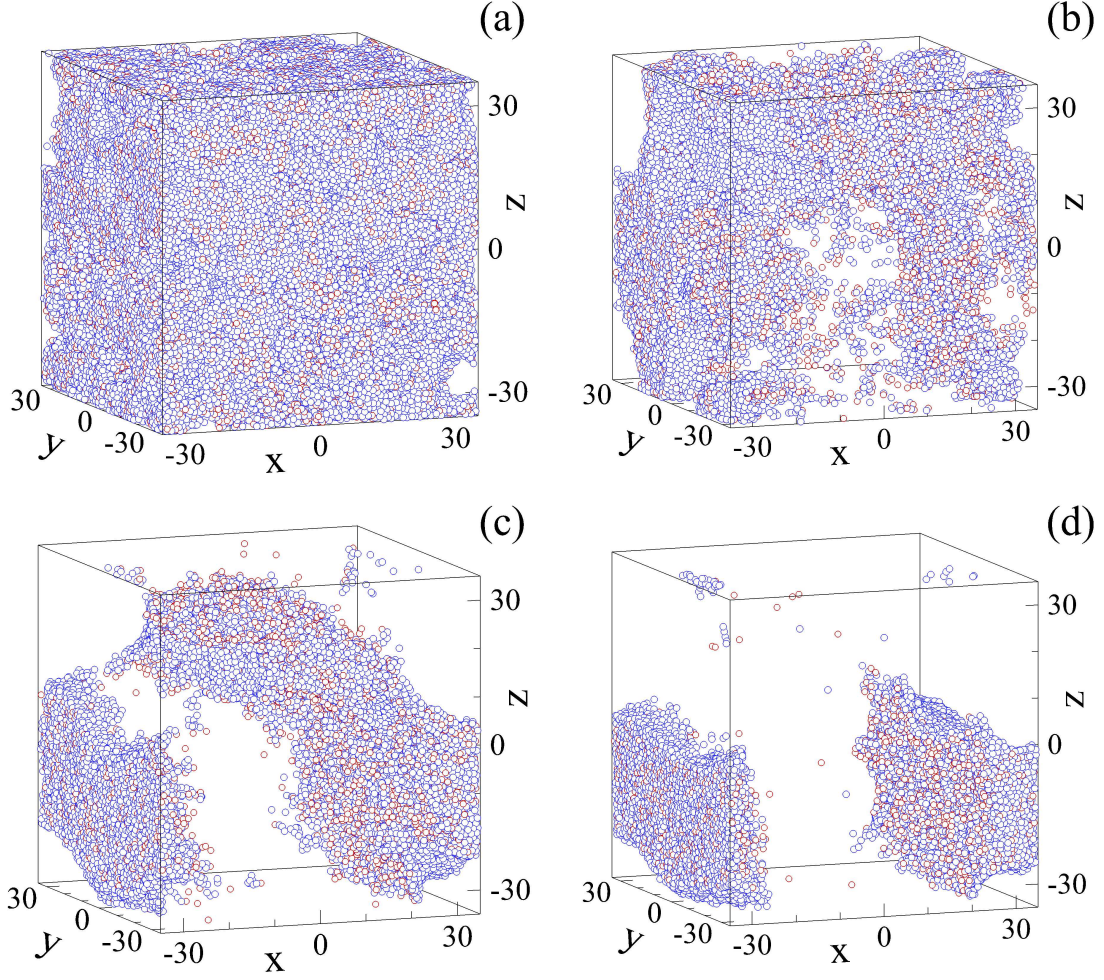


FIG. 11: (Color online) The positions of mobile atoms with displacements during one cycle greater than 0.6σ for the cycle numbers (a) 1, (b) 10, (c) 100, and (d) 500. The strain amplitude is $\gamma_0 = 0.10$. The same data as in Fig. 7.

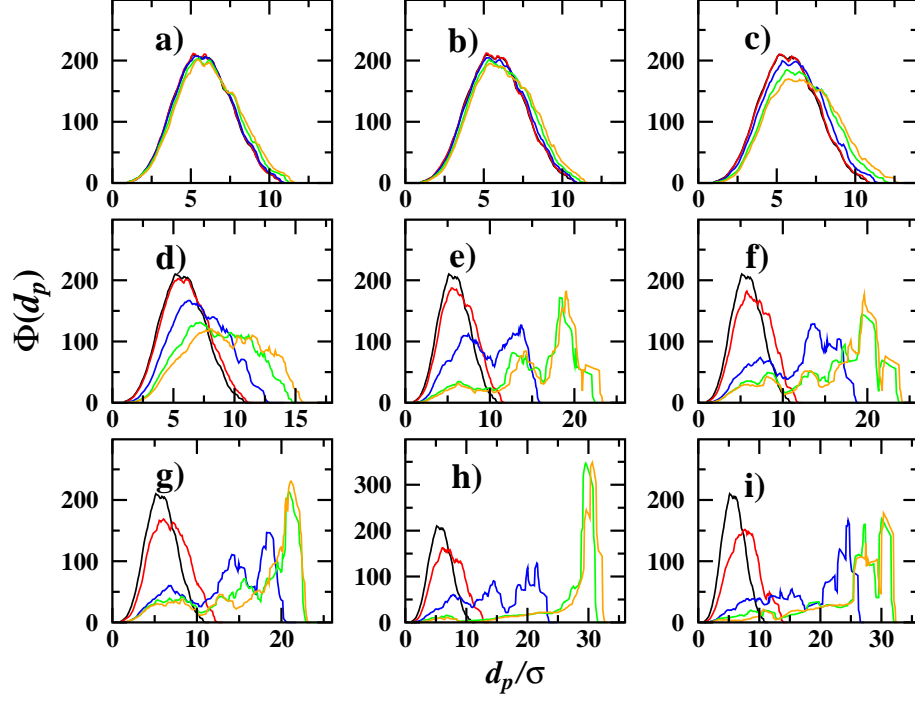


FIG. 12: (Color online) The distributions of pore sizes for the strain amplitudes, γ_0 : (a) 0.0, (b) 0.01, (c) 0.02, (d) 0.04, (e) 0.06, (f) 0.07, (g) 0.08, (h) 0.10, and (i) 0.12. The cycle number is indicated by: 0 (black), 1 (red), 10 (blue), 100 (green), and 500 (orange). The data sets were averaged over 20 points for clarity. The black curves are the same in all panels.

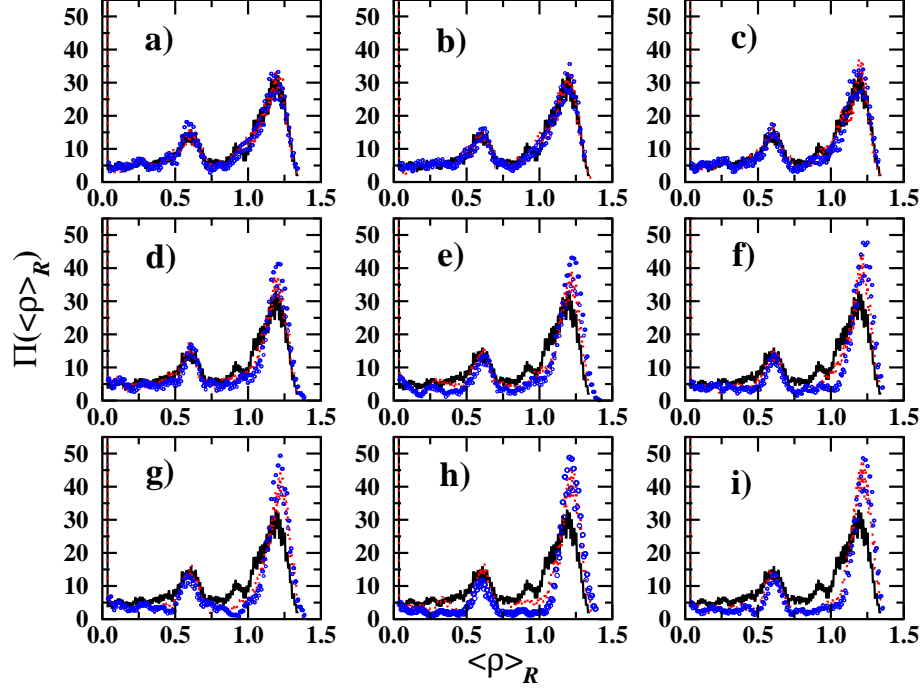


FIG. 13: (Color online) The local density distribution functions, $\Pi(\langle \rho \rangle_R)$, for the strain amplitudes, γ_0 : (a) 0.0, (b) 0.01, (c) 0.02, (d) 0.04, (e) 0.06, (f) 0.07, (g) 0.08, (h) 0.10, and (i) 0.12. The bin size is fixed to $\langle \rho \rangle_R^{\max}/400$ and each data set was averaged over 20 points. In each panel, the colorcode for the cycle number is: 0 (solid black line), 100 (dashed red line), and 500 (open blue circles).

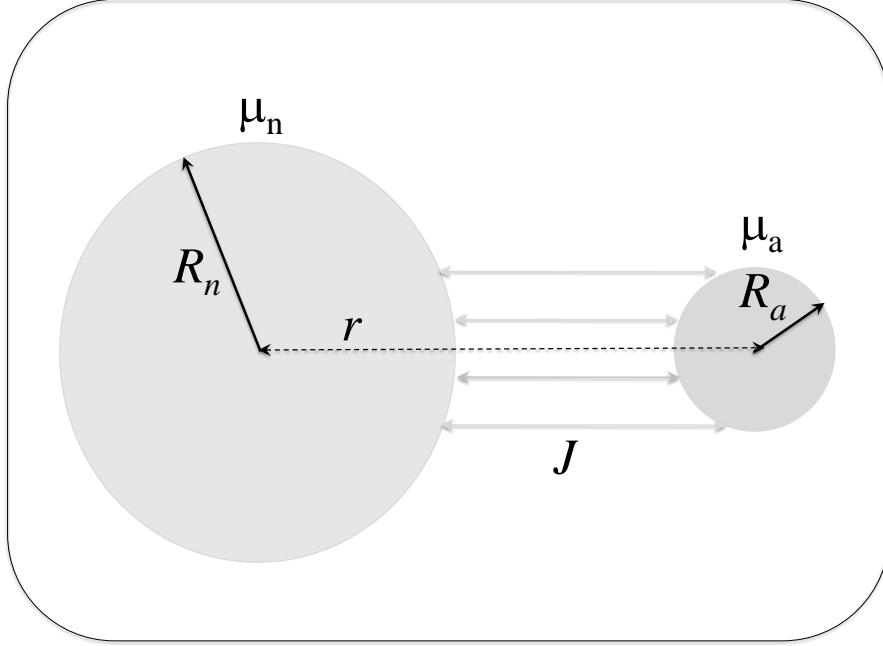


FIG. 14: A schematic illustration of the pore annihilation mechanism. A small pore with radius, R_a , located in a vicinity of a neighboring pore with radius, R_n , undergoes an instability due to a temperature increase or an external mechanical perturbation. Atomic rearrangements occur due to the gradient of chemical potential, $\nabla\mu$. The structural rearrangements, leading to the small pore annihilation, are described by the atomic current flux into the pore, J , defined by the Fick's law.